Mongolian Geoscientist

Original Article

Velocity analysis of a lateral wave

Tsogtbaatar Amarsaikhan[*] [iD], Motoyuki Sato [iD]

[*]*Center for Northeast Asian Studies, Tohoku University, 41 Kawauchi, Aoba-ku, Sendai, Miyagi, 980-8576, Japan*

Corresponding author: tsogtbaatar.amarsaikhan.b7@tohoku.ac.jp, ORCID: 0000-0003-1285-8621

ARTICLE INFO

ABSTRACT

In practice, the reflected EM signal cannot be clearly observed in GPR data due to the high water content and other reasons. However, the antenna coupling signal through the ground interface is dominated in all the GPR measurements. This direct coupling signal that travels through the ground interface is called a lateral wave. The properties of the lateral wave directly depend on the subsurface properties, especially electrical parameters. We have numerically analyzed a lateral wave and its velocity. Subsequently, the relationship between lateral wave and dielectric permittivity was determined by polynomial regression. Analytically, it is challenging to analyze a lateral wave due to the parameters that can influence wave propagation. Antenna characteristics, surface roughness, etc need to be considered. Numerically, we designed a GPR system with a subsurface layer and observed a lateral wave. This numerical analysis can give a chance to use a lateral wave for near-surface soil water content. This analysis gives a more precise estimation of surface water content. Moreover, we analyze the antenna height effect that influences radar signals. We numerically observed that the GPR signal is highly affected by antenna height. The antenna height effect depended on the wavelength of the applied electromagnetic wave. By adjusting the antenna height, the unobservable GPR signal can be clearly detected.

Keywords: FDTD simulation, electromagnetic wave, CMP,

INTRODUCTION

Surface soil water is one of the most important parameters in near-surface geology. The soil water content is highly variable both in space and time, especially in a range of processes. Moreover, topography, precipitation, evaporation, geology, and vegetation also control water content. Surface water keeps the sustainability and underground water balance. An advanced understanding of near-surface water content is useful for many applications, such as agriculture, sedimentary geology, hydrogeology, and engineering.

While in geophysical surveys, GPR is typically used because of the permittivity nature of the soil, and its high resolution at depth for a near-surface. Recently, GPR has proven a viable tool for determining near-surface layered structures. The conventional methods require a huge number of closely spaced measurements to determine the spatial distribution of soil water content in a field. Not only these conventional methods are time-consuming, but they also disturb the soil structure quite a lot. GPR

measurement can provide a velocity of EM waves, including lateral waves and reflected waves that can be used for estimating near-surface water content. Using the velocity of reflected EM waves, the water content of the layered structure can be determined in terms of the velocity of EM waves. After the velocity is converted to the dielectric permittivity, the volumetric water content is estimated by using one of the empirical equations describing the relationship between the water content and dielectric permittivity.

In general, two different approaches are used to map soil water content with a surface GPR method. The first approach is based on reflected EM waves. This method requires reflected signals that can be used for the velocity analysis technique. Reflected EM waves can be used for estimating water content when a reflected wave is observed. In some field measurements, it is very common that reflected EM waves are not observed because of attenuation and inhomogeneity. The second approach is to use lateral EM waves for estimating surface water content. In this method, the most challenging thing is to define a relation between the velocity

of a lateral wave and water content. The main objective of this work is to develop and evaluate an optimistic relation of the lateral wave for surface water content. In this research, the numerical calculation and field observations will be presented.

LATERAL WAVE PROPAGATION

The particular type of electromagnetic wave is generated on or near the boundary between air and earth (soil, lake water, sea water) or the sea floor and sea water is generally known as a lateral wave (King et al., 1992). When the transmitter antenna is positioned close to a dielectric half-space (ground surface), a lateral wave is excited in addition to the direct coupling wave as shown in Fig.1. Both wave propagations that are traveled in air and ground have spherical wavefronts. Airwave travels the air medium at the velocity of the EM wave in a vacuum (0.3 m/ns). The EM wave travels through the dielectric medium (soil) at a velocity that is dependent on the dielectric permittivity. The propagation wavefront of a lateral wave depends on the dielectric contrast between the air and ground layer. When boundary conditions
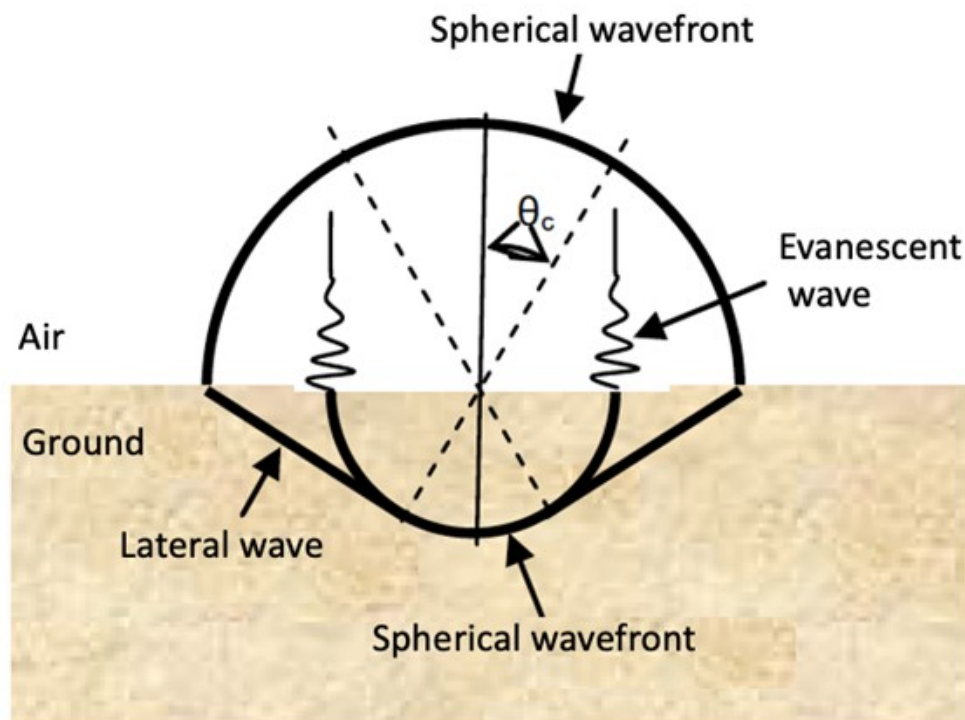

Fig. 1. Physical interpretation: spherical wave, lateral wave, and evanescent wave (Shavit and Rosen,1995)

are satisfied, a lateral wave is added to the incident, reflected, and refracted waves (Zou et al., 2020). Lateral wave is typically acquired in both common offset and Common Mid-Point (CMP) measurement.

As shown in Fig. 1, a lateral wave can spread a tangent waveform connecting both spherical waves traveling in air and ground along the boundary. Because of the constant velocity of air, the velocity of a lateral wave only depends on subsurface electrical properties. The amplitude of a lateral wave attenuates as $1/\rho^4$ (ρ–the distance to the source) and its loss is independent of subsurface material (Annan, 1973). The energy loss of the lateral wave is obviously larger than the airwave and other waves due to the continuous shedding of energy away from the subsurface. However, the amplitude of the lateral wave can exceed the amplitude of the spherical wave in large-distance propagation. The propagation of lateral waves can be considered as the distance between Tx antenna and Rx antenna (Annan, 1973). Due to the velocity of the lateral wave depending on the electrical properties of subsurface material, the observed velocity of the lateral wave can be used to estimate the EM properties of the subsurface medium. The velocity of the lateral wave can be used to

estimate the dielectric properties of the medium based on the appropriate approximation.

In a short antenna separation, lateral and direct coupling signals are mixed in a received signal. The multi-offset measurement can give a chance to observe the separated lateral wave from the direct coupled wave. Due to the applied GPR frequency, a direct coupled wave, lateral wave, and reflected wave are commonly mixed in short antenna separation. When antenna separation increases, all the GPR signals are separated. Fig. 2 shows some of the field data acquired by the CMP method in Bulgan province, central Mongolia. The solid black line overlapped in the hyperbolic reflection events. The simulated hyperbolic curve was drawn using trial velocities.

At the very beginning of the antenna separation, the waveforms of the lateral wave and direct couple wave consist of each other. In order to separate the signals, antenna separation must be kept at enough distance. Thus, we can individually pick an arrival time of the lateral wave. Knowing antenna separation, we can clearly determine the velocity of the lateral wave. However, the velocity of the lateral wave does not only depend on the subsurface layer but also on the GPR system, surface roughness, and vegetation cover (de Coster and Lambot, 2019). The one of advantages of multi-offset
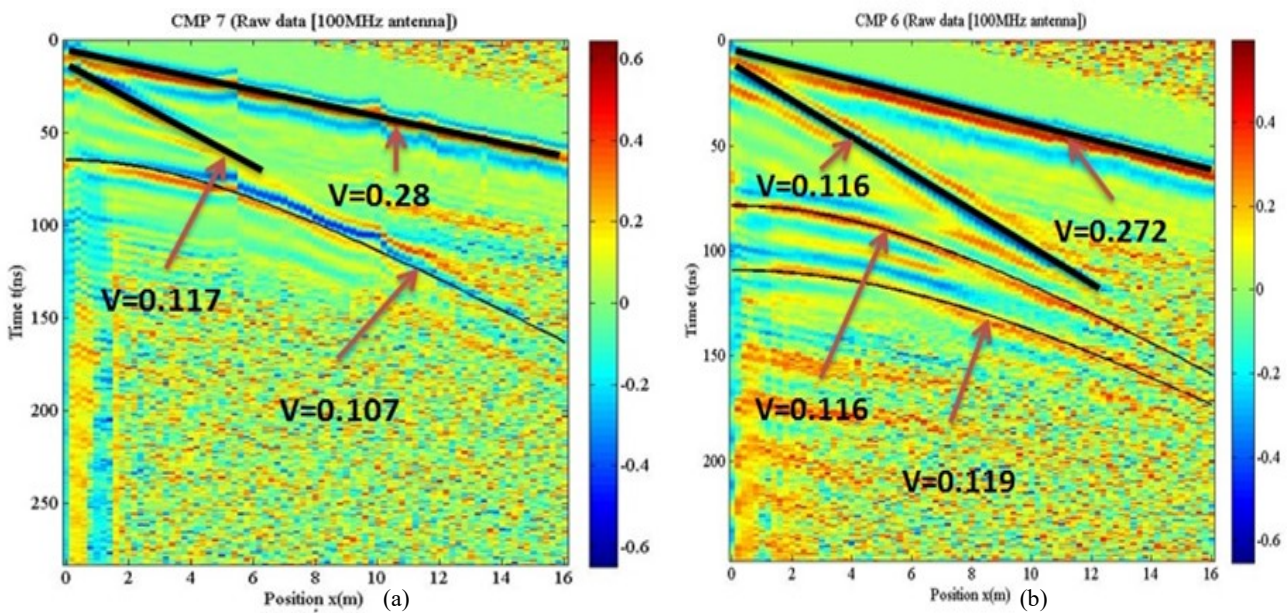

Fig. 2. The CMP sounding data with profiles obtained in Bulgan province, central Mongolia show the results of velocity analyses

measurement is to interpret the lateral waves (Zou et al., 2020). In most GPR systems, the penetration depth of the lateral wave is around tens of centimeters. Thus, the lateral wave can play important role in shallow surface analysis. Some researchers have done research work on the lateral wave to estimate soil water content (Gerhards et al., 2008).

Basically, the lateral wave propagates along the boundary between layers. Due to the slower velocity, it is recorded after a direct coupled wave. When a reflector exists, the reflected and refracted EM waves are observed in GPR data.

METHOD
Velocity analysis of the lateral wave

To extract subsurface information using the lateral wave, an amplitude and a velocity of the lateral wave can be used. In an ideal case, the signal amplitude of GPR indicates the reflection coefficient of the reflector boundary. However, there are some factors that influence the amplitude. The signal amplitude of the GPR signal can be expressed as the following equation (Bradford and Deeds, 2006):

$$Amp_{obs} = \frac{A_T \cdot A_R \cdot C_T \cdot C_R \cdot T}{G} \cdot r \cdot e^{-\alpha \rho} \cdot Amp_{sou} \quad (1)$$

where, A_T and A_R are the radiation pattern of the Tx antenna and Rx antenna, respectively. T -is transmission loss across the boundaries in the overlay. G -is the geometric spreading factor (Green function) and r -is the reflection coefficient. Amp_{sou} -is the amplitude of the source signal. ρ -is the propagation path of the wave. C_T and C_R are the coupling factor of Tx antenna and Rx antenna. Each of these parameters is a function of applied frequency, dielectric permittivity, electrical conductivity, magnetic permeability, and so on. Zou et. al. (2020) have used the amplitude of the lateral wave to detect a debonding of the asphalt airport pavement.

In this study, we used the velocity of a lateral wave and then find a relation between the velocity of a lateral wave and surface water content. Fig. 3 shows the lateral waves observed in CMP measurement. We can observe a lateral wave in the CMP method as a linear, because of its constant velocity. In the GPR profile of the CMP measurement, we can only see the lateral wave and direct coupling waves, as shown in Fig. 3.
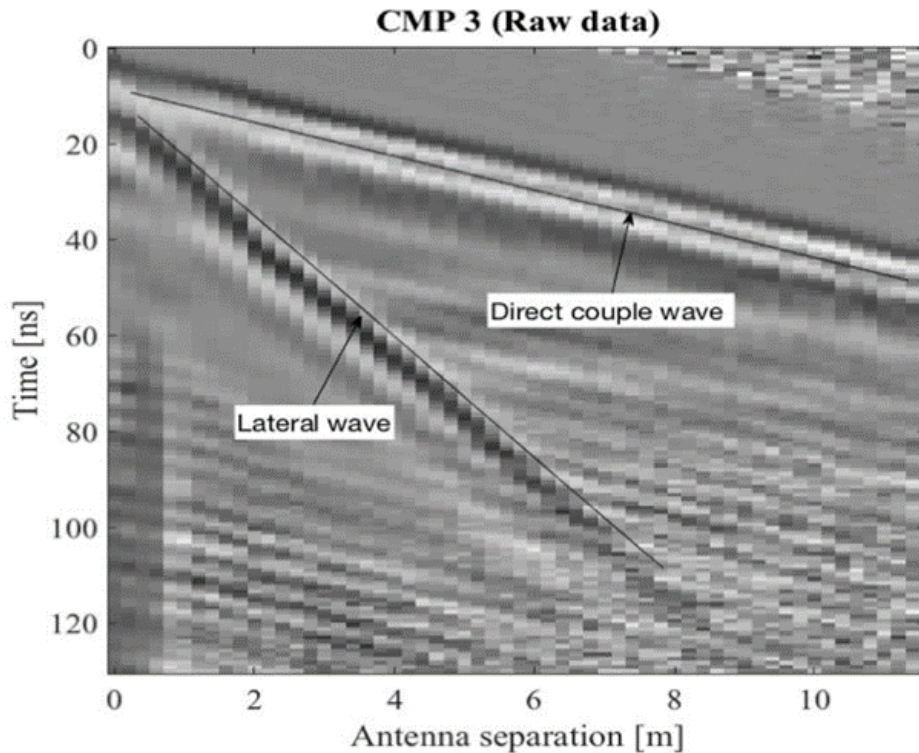
Only multi-offset (CMP) measurement can give

Fig. 3. GPR profile of CMP dataset

(a)   (b)
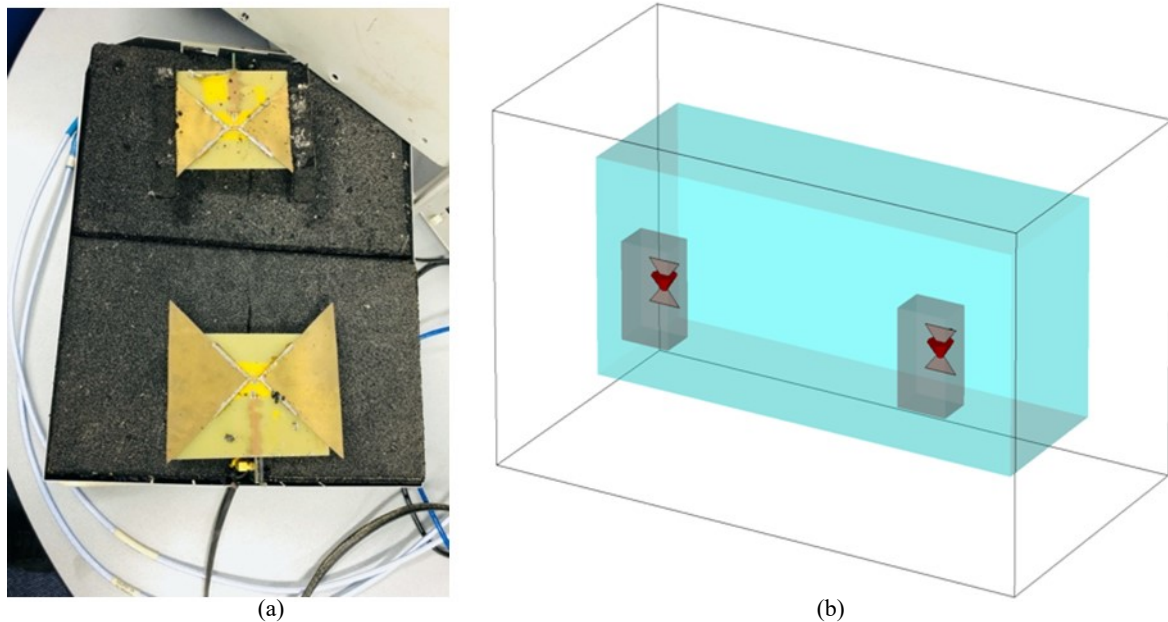
Fig. 4. GPR antenna (a) Real structure (b) Designed model for FDTD

a velocity of the lateral wave. Without validation of the lateral wave velocity, we cannot estimate the velocity of the lateral wave from a common offset method. Only the lateral variation can be observed from common offset data. With CMP measurement along the survey lines, we can have a velocity of the lateral wave profile along a survey line. This gives a chance to estimate surface water content on a large scale. In order to convert the velocity of the lateral wave into water content, we need to find a relation between velocity and dielectric permittivity. Due to the uniqueness of the lateral wave, we cannot directly calculate the velocity of the lateral wave as a normal wave propagation.

In order to find a relation between the velocity of the lateral wave and the dielectric permittivity of a medium, we numerically conducted CMP measurement using the 3D FDTD (Finite Difference Time Domain) method. Antennas were designed as same as RAMAC/GPR with 500 MHz shielded antenna.

Numerical simulation of CMP measurement
By using CST Microwave studio software, we design a GPR system as same as RAMAC 500 MHz antenna. To have the same performance as the GPR signal, the bow-tie antenna was used for the numerical simulation as shown in Fig. 4.

By changing the antenna separation, the lateral waves were separated at each acquired data.
The dimension of the modeled single layer is 1500 mm 600 mm 500 mm. Fig. 5a shows the CMP profile of the simulation data using the modeled structure. In order to estimate water content, we only focused on the velocity of the lateral waves. By changing the antenna separation, we can see the amplitude decrease and the time delay as shown in Fig. 5b. To pick up the arrival time of a lateral wave, we gradually changed the electrical parameter of the modeled layer. For estimating the velocity of a lateral wave, we only changed the dielectric permittivity of the layer to a range from 10 to 20. As shown in Fig. 5a the amplitude of the lateral wave exceeds the direct couple wave at all the antenna separations. The EM absorbing structure used in the simulation model affected the amplitude of the direct coupling wave. Therefore, the major signal observed in the CMP profile is the lateral wave.

To check the separation dependency of a velocity and an amplitude, these parameters were calculated for each separation as shown in Fig. 6. The amplitude significantly decreased by the changing separation. However, the velocity of the lateral wave is quite stable for changing antenna separation.
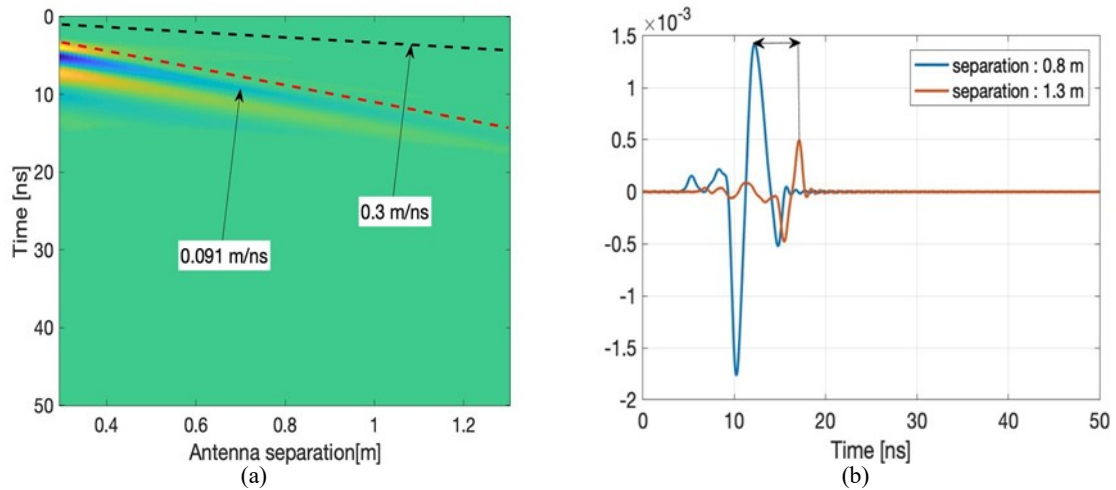
(a)

(b)

Fig. 5. (a) CMP profile (b) Selected traces
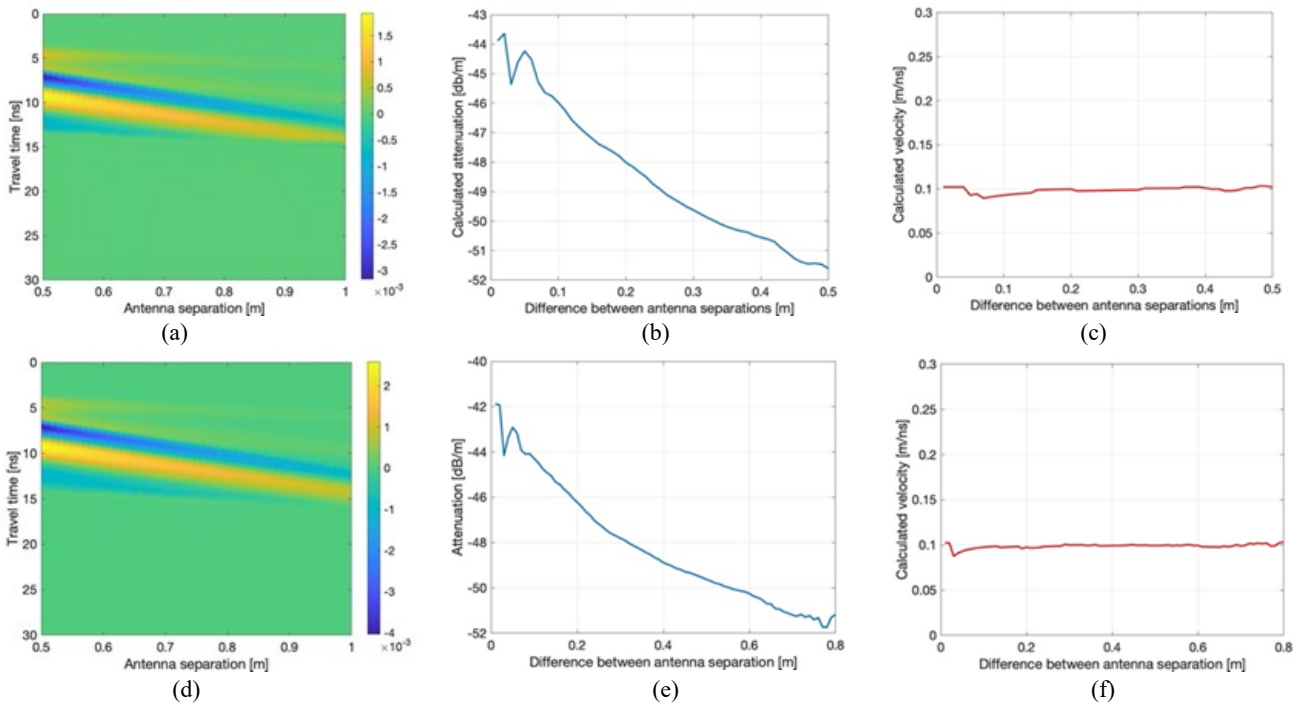

(a)

(b)

(c)

(d)

(e)

(f)

Fig. 6. Lateral wave analysis for CMP data (ε_r=10, σ_1=0.01, σ_1=0.001) (a, d) CMP profile (b, e) Calculated attenuation (c, f) Calculated velocity

The velocity analysis of the lateral wave is to find a relationship between the lateral wave and the water content. Thus, we numerically analyzed the velocity of the lateral wave for changing the dielectric permittivity of the layer. The following figures show the CMP profile for the numerical calculation of each dielectric permittivity (Fig. 7). By gradually changing the dielectric permittivity of the layer, the corresponding velocity of all the measurements

has been observed. In statistical analysis, we use the velocity of the lateral waves acquired as an independent variable.

The separation of the antenna was increased from 0.3 m to 1.3 m, and an increment of 4 cm. The time window was adjusted at 50 ns with 1024 sampling points. The velocity of the lateral waves was calculated using the arrival time at different antenna positions. Fig. 8 shows the amplitude and phase angle information of the
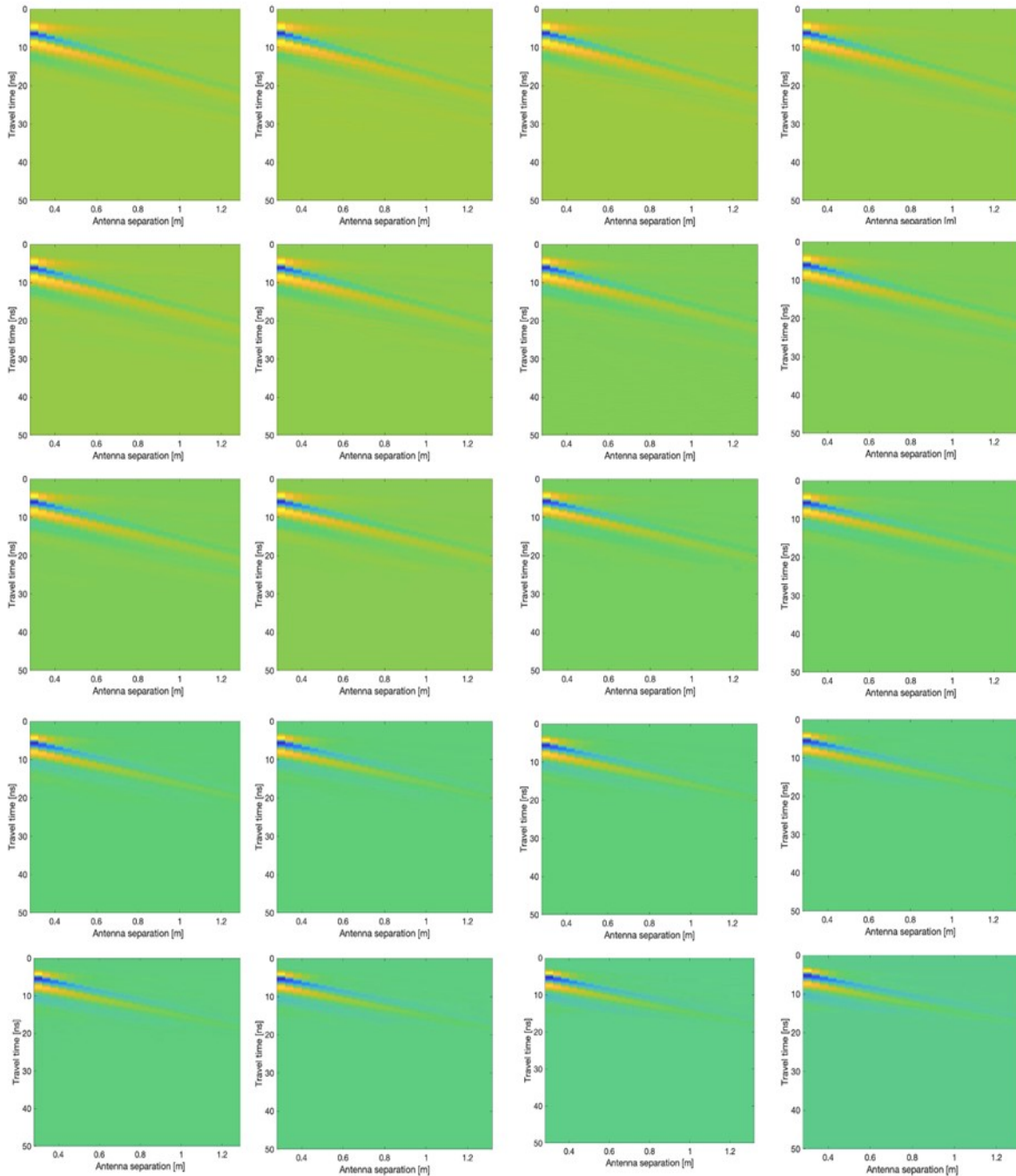
Fig. 7. CMP profiles with a dielectric permittivity range (from ε_r=10 to ε_r=20) with 0.5 increment

simulated CMP data. High amplitude components dominate the frequencies of 100 MHz to 500 MHz.

Antenna height effect on GPR signal
Ideally, the GPR system fully contacts with ground surface. However, both Tx and Rx antennas cannot fully touch the ground surface

due to the surface roughness and antenna properties. In the numerical models, we tried to evaluate how antennas affects received signals, especially the reflected signals. Based on the numerical models, reflected signal amplitudes were observed depending on the antenna height for each CMP configuration. Sato et al. (2015) evaluated that most of the electromagnetic
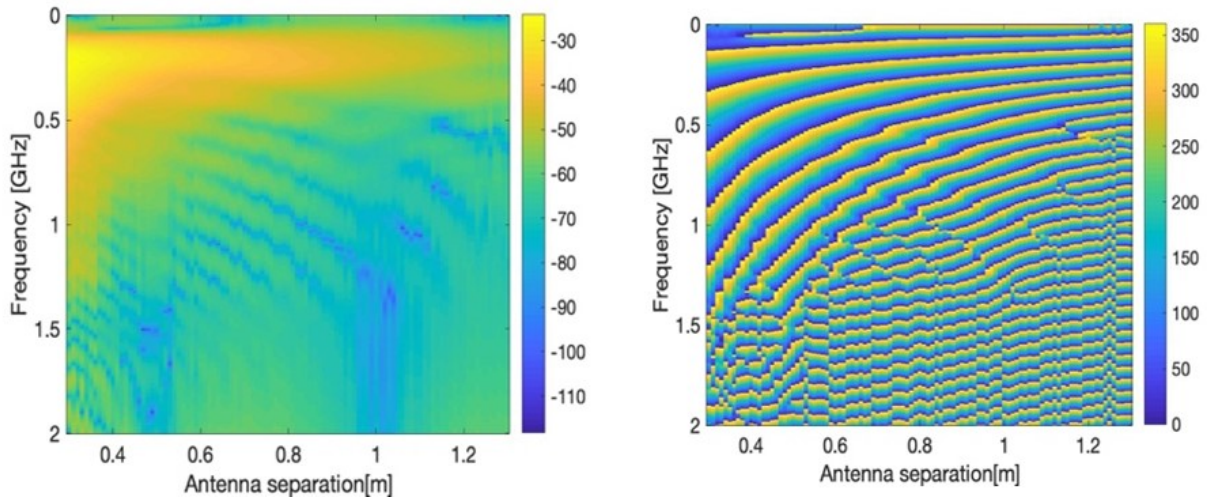
Fig. 8. (a) Amplitude (S21 parameter) (b) Phase angle: unwrapped (c) Phase angle: wrapped
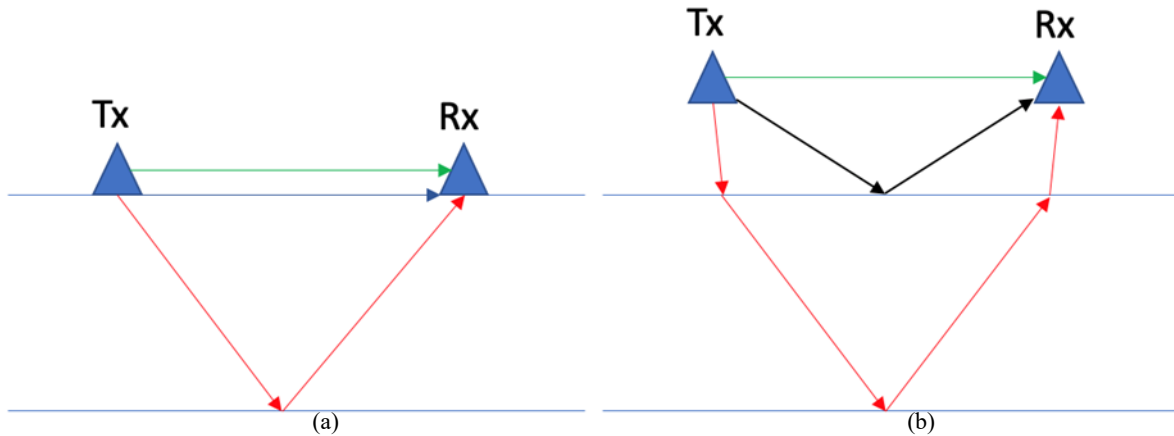

Fig. 9. (a) Conventional GPR system (b) Air-launched GPR system

energy from the GPR antennas placed at wavelengths 1/10 from the ground surface is transmitted to the soil, but not to the air, due to waves trapped along the boundaries, and this phenomenon does not occurred when the antenna height is greater than 1/3 of the wavelength. We have increased the antenna height much lower than the wavelength of the applied EM wave. By gradually increasing the antenna height, the CMP dataset were obtained for each antenna height from 0 mm to 16 mm. The analysis focused not only on the reflected waves, but also on the lateral waves. If we increase the height of the antenna much larger than the wavelength of the applied EM wave, we cannot generate lateral waves. Fig. 9 shows the principle of the GPR launched in the air. The ground medium consists of two horizontal layers that differ from electrical parameters. We observed that the variation of the GPR signals included the direct couple, the lateral wave, and the reflected wave of each antenna height. Both the dielectric permittivity of first (depth: 3 m) and second layer were defined to be ε_r=4 and ε_r=10. Moreover, we considered electrical conductivity of both layers which were σ=0.0001 and σ=0.001, respectively. The numerical simulation was conducted on FDTD method. Fig. 10 shows a time domain signal with different antenna offsets.

Changing the height of the antenna form the 0 mm to 16 mm, direct couple waves, lateral waves, and reflected waves were observed by arrival time and amplitude. We observed waveform changes for a lateral wave and
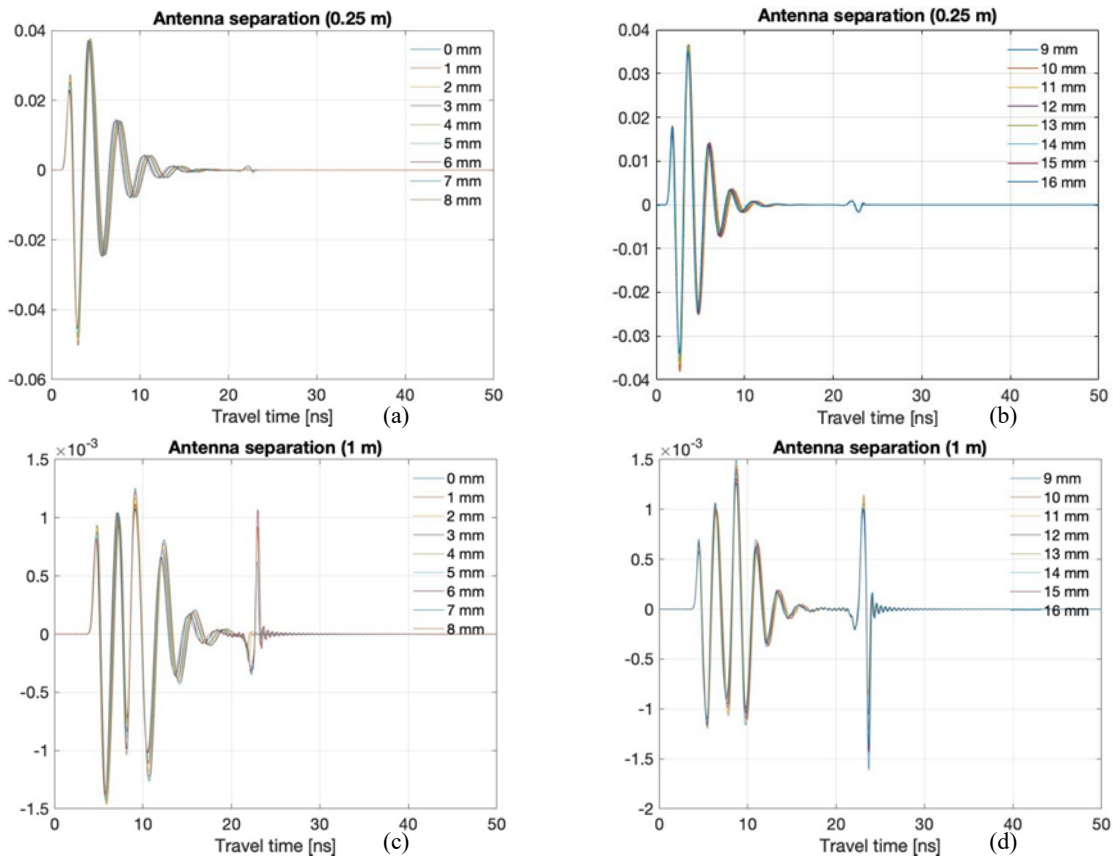
Fig. 10. Time domain signals of different antenna heights (a, b) 0.25 m (b, d) 1 m.
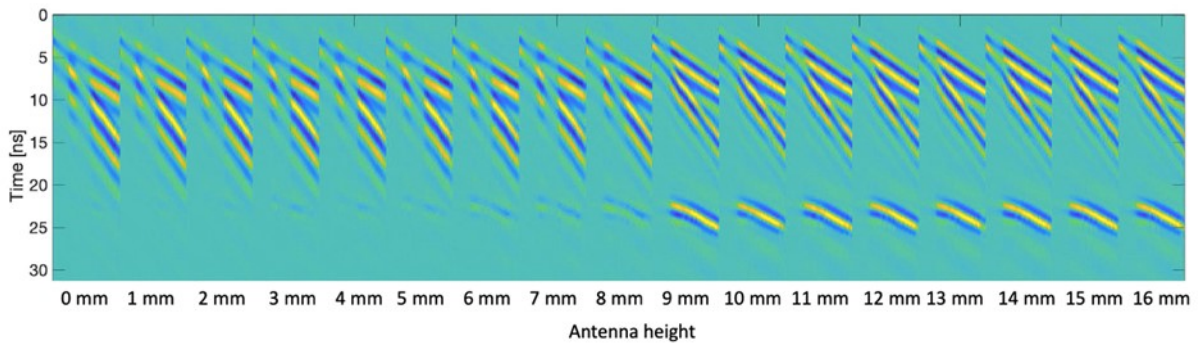

Fig. 11. GPR profiles of CMP measurement with different antenna height

reflected waves. When comparing reflected signals for different antenna separation, we observed that the amplitudes of the reflected signals were increased above 8 mm. In short antenna separation (0.25 m), the amplitude of the reflected signal is much smaller than the amplitude of coupling signal. However, we could observe high amplitude reflected waves in long antenna separation (1 m), as shown in Fig. 10d. The GPR profiles with different antenna heights. Conventional signal processing was applied to all the CMP datasets (Fig. 11).

Note that in the FDTD numerical simulation model, the antenna packaging was not considered. Thus, the result of the in this numerical method can be used to designing unshielded antenna systems.

Curve fitting model

By obtaining the velocities of the lateral wave using the numerical simulation method, a curve fitting model can be applied for velocity data as
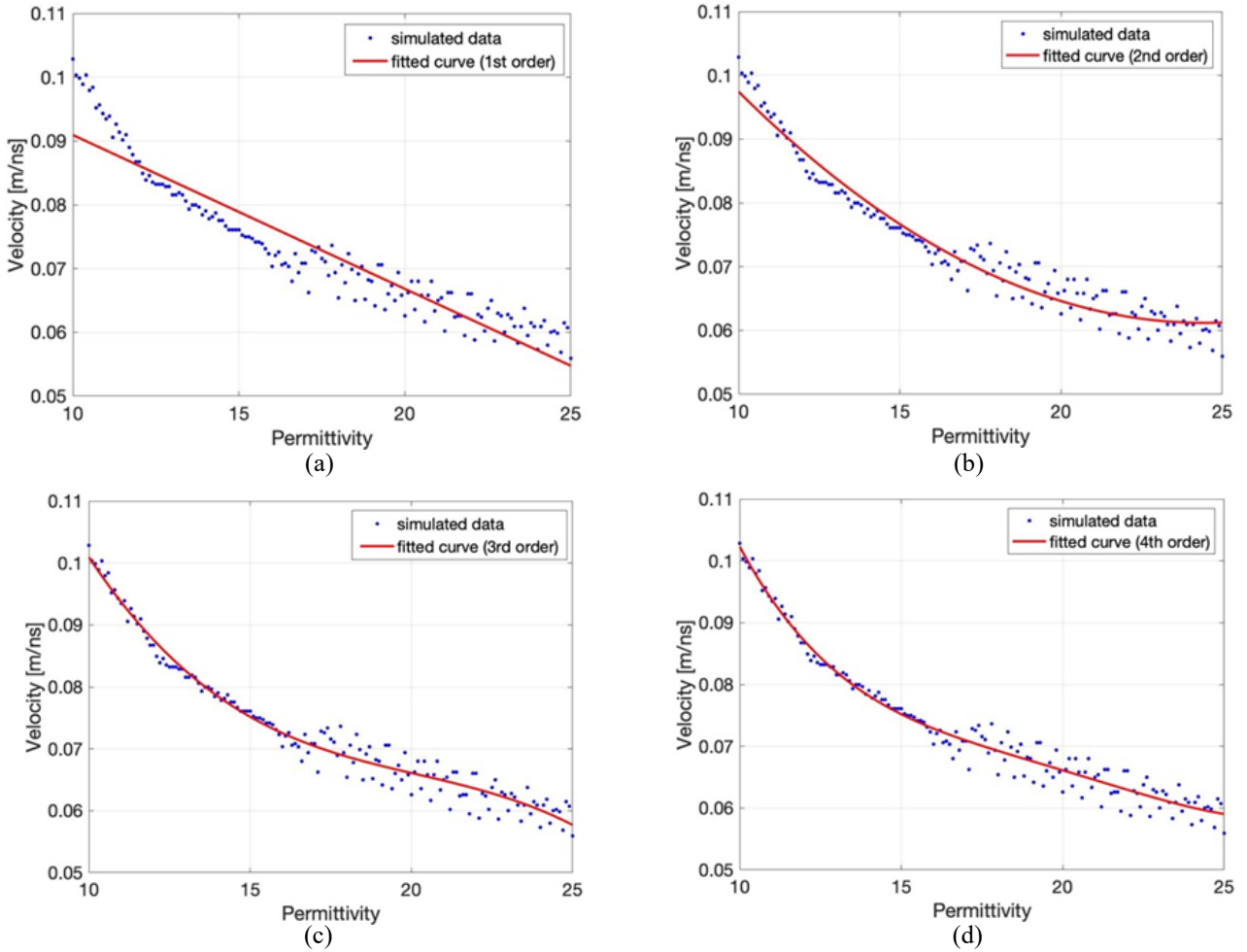
Fig. 12. Polynomial models of the lateral wave (a) n=1 (b) n=2 (c) n=3 (d) n=4

independent variables. To fit and get the optimal relation between the velocity of the lateral wave and dielectric permittivity, the number of fitting models were applied to the velocity data.

Polynomial regression models for the one independent variable are given by the following equation (2):

$$y = \sum_{i=1}^{n+1} p_i x^{n+1-i} \qquad (2)$$

where, ***n+1*** -is the order of the polynomial, is the degree of the polynomial. The order gives the number of coefficients to fit, and the degree gives the highest power of the predictor variables. For example, a third degree of polynomial is given by Eq. (3):

$$y = p_1 x^3 + p_2 x^2 + p_3 x + p_4 \qquad (3)$$

Basically, polynomial models are used when a simple empirical model is required. In this case, we use the polynomial model to find the optimal model to convert velocity into dielectric parameters. However, the polynomial model do not fit all the GPR data due to the GPR system and surface roughness, etc. Using a polynomial model, we can predict the dielectric permittivity using a range of velocity data. We obtained velocity data from the FDTD simulations at dielectric permittivity from 10 to 20. Fig. 12 shows the fitted curves with different degrees of the polynomial.

In order to have a more optimal model and predict dielectric permittivity, the curve fitting models were extended in several ways. First, we increased a polynomial degree from 1 to 4. It is
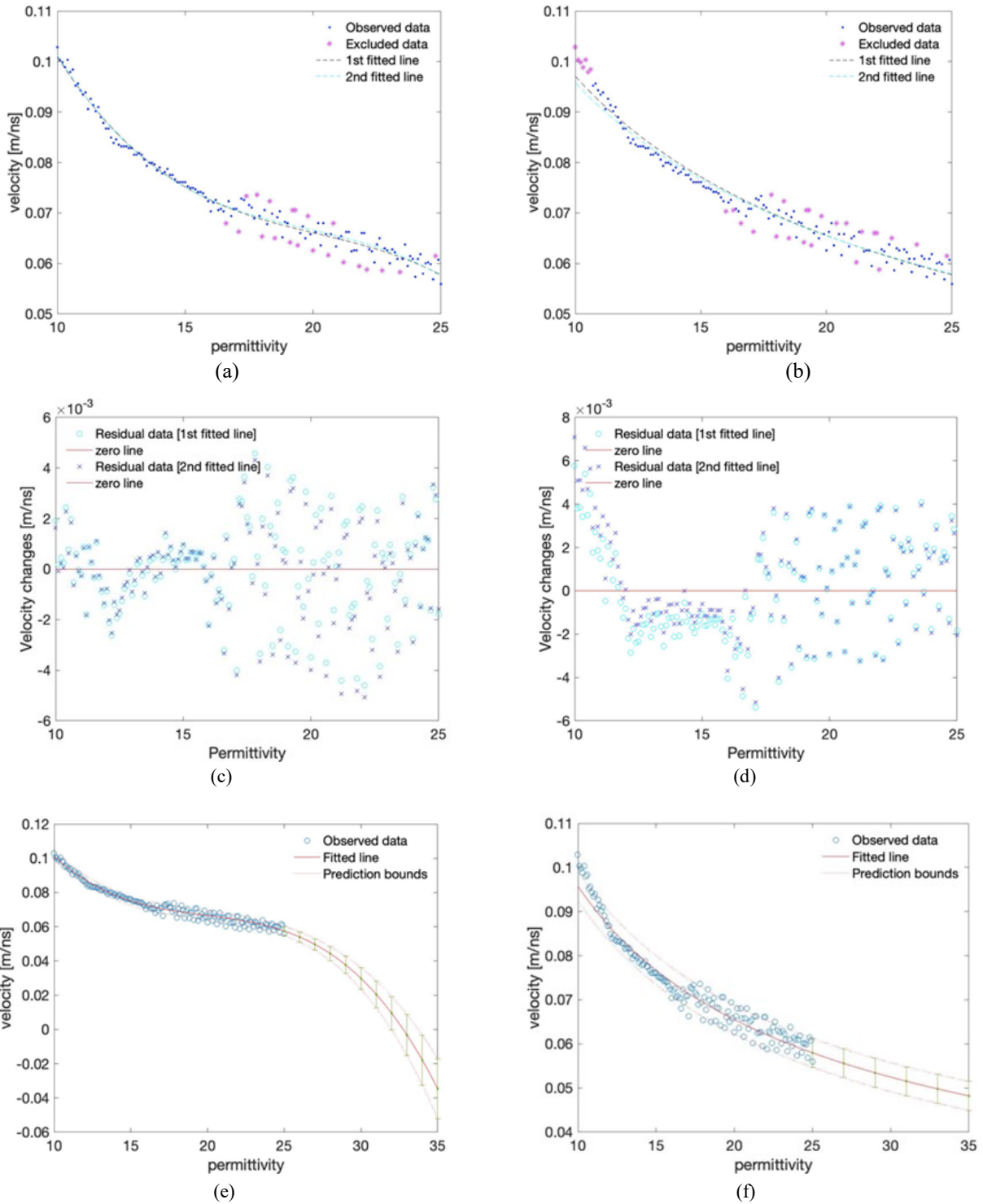
Fig. 13. Extended polynomial models (a) 3rd degree polynomial (b) Formula based model (c) Residual data (d) Residual data (e) Predicted data (f) Predicted data

Table 1. Polynomial coefficients of the estimated functions

$f(x) = p_1 x^5 + p_2 x^4 + p_3 x^3 + p_4 x^2 + p_5 x + p_6$						
Degree	p_1	p_2	p_3	p_4	p_5	p_6
1	0	0	0	0	-0.002412	0.1151
2	0	0	0	0.000174	-0.008501	0.165
3	0	0	$-2.132 \cdot 10^{-5}$	0.001293	-0.02736	0.2665
4	0	$1.93 \cdot 10^{-5}$	-0.0001565	0.004767	-0.06544	0.4193
5	-	$9.46 \cdot 10^{-6}$	-0.0000414	0.009076	-0.1009	0.5326

Table 2. Polynomial models

Model 1	Model 2
$f(x) = ax^3 + bx^2 + cx + d$	$f(x) = \dfrac{a}{x^b} \qquad \left(v = \dfrac{c}{\sqrt{\varepsilon_r}} \right)$
a=-0.0000241	*a=0.3384*
b=0.00143	*b=0.5481*
c=-0.0297	
d=0.2786	

very clear that the relation between dielectric permittivity and velocity of a lateral wave is a non-linear function. Fig. 13 shows the fitted
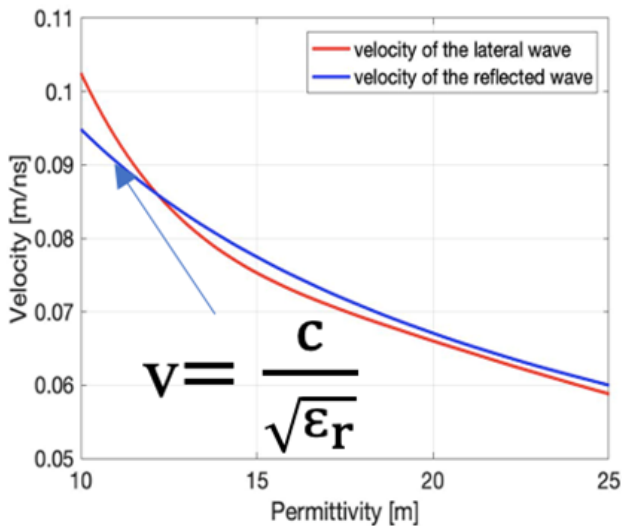

Fig. 14. The velocity comparison of the lateral wave and the reflected wave

curves with the predicted data range. To have a predicted data for the range of permittivity exceeded the simulation range, the polynomial analysis was used to calculate a dielectric permittivity with a prediction bound.

As shown in Figs. (13e and f), the predicted data with corresponding bounds are quite different. Thus, we considered an optimal relationship based on the equation that is used for ground wave velocity. Table 2 shows the coefficients of estimated equations. In polynomial Model 2, as shown in Fig. 13b, we can have a more reliable model.

Fig. 14 shows the comparison of the spherical wave and the lateral wave that we obtained from numerical calculation.

DISCUSSION

Research focuses on the application of GPR technology to advanced signal processing technologies to quantitatively characterize subsurface geology and environmental studies. The main purpose is to precisely estimate the velocity of electromagnetic waves and then calculate the hydrogeological parameters. The conventional CMP method is faced with a signal processing step problem. The analysis of lateral wave is introduced by the numerical simulation. In some field experiments, due to the electrical properties of the substrate and the performance of the GPR system, the reflection waves are not observed. However, the antenna

coupling signal is always dominated by radar signal.

CONCLUSION

The coupling signal through the surface interface strongly depends on subsurface properties, vegetation cover, surface roughness, and antenna characteristics. To find a relationship between the dielectric permittivity of the near-surface and the observed velocity of the lateral wave, we carried out numerical measurements of the CMP using the FDTD method. By conducting numerous CMP measurements, which changed the dielectric permittivity of the near-surface, the velocity of the lateral waves was calculated. Afterwards, polynomial regression was applied to find a relationship. However, the estimated relationship between the dielectric permittivity and the velocity can only fit the designed antenna properties. In our case, we have designed a commercial 500 MHz RAMAC antenna. Thus, we can design any antenna for lateral wave analysis. Consequently, the roughness of the surface must be taken into account in the numerical calculation.

ACKNOWLEDGEMENTS

REFERENCES

Annan, A.P. 1973. Radio Interferometry Depth Sounding: Part I -Theoretical Discussion. Geophysics, v. 38(3), p. 557-580. https://doi.org/10.1190/1.1440360

Bradford, J.H., Deeds, J.C. 2006. Ground-penetrating radar theory and application of thin-bed offset-dependent reflectivity. Geophysics, v. 71(3), K47. https://doi.org/10.1190/1.2194524

de Coster, A., Lambot, S. 2019. Full-Wave Removal of Internal Antenna Effects and Antenna-Medium Interactions for Improved Ground-Penetrating Radar Imaging. IEEE Transactions on Geoscience and Remote Sensing, v. 57(1), p. 93-103. https://doi.org/10.1109/TGRS.2018.2852486

Gerhards H., Wollschläger, U., Yu, Q., Schiwek, P., Pan, X., Roth, K. 2008. Average Soil-Water Content with Multichannel Ground-Penetrating Radar. Geophysics, v. 73(4), p. 15-23. https://doi.org/10.1190/1.2943669

King, R.W.P., Owens, M., Wu, T.T. 1992. Lateral Electromagnetic Waves. Theory and Applications to Communications, Geophysical Exploration, and Remote Sensing. 1st ed, New-York, Springer-Verlag, ISBN: 978-1-4613-9174-6

Sato, M., Takahashi, K., Asaya, Y., Iitsuka, Y. 2015. Radiation of electromagnetic wave from an antenna placed close to a boundary of materials, Simulation of GPR antenna. IEICE Technical Report, EMT2015-20, v. 115(141), p. 65-70.

Shavit, R., Rosen, E. 1995. Lateral wave contribution to the radiation from a dielectric half medium. IEEE Transactions on Antennas and Propagation, v. 43(7), p. 751-755. https://doi.org/10.1109/8.391154

Zou, L., Yi, L., Sato, M. 2020. On the Use of Lateral Wave for the Interlayer Debonding Detecting in an Asphalt Airport Pavement Using a Multistatic GPR System. IEEE Transactions on Geoscience and Remote Sensing, v. 58(6), p. 4215-4224. https://doi.org/10.1109/TGRS.2019.2961772